

1 **Ionospheric influence on the seismo-telluric current related to electromagnetic**
2 **signals observed before the Wenchuan $M_S=8.0$ earthquake**

3
4 Mei Li^{1,2}, Handong Tan² and Meng Cao²

5
6 (1) China Earthquake Networks Center, China Earthquake Administration, No.5,
7 Sanlihe Nanhengjie, Xicheng District, 100045 Beijing, China.

8 (2) China University of Geosciences, No.29, Xueyuan Road, Haidian District, 100083
9 Beijing, China.

10
11 Corresponding author: Handong Tan, China University of Geosciences, No.29,
12 Xueyuan Road, Haidian District, 100083 Beijing, China. (thd@cugb.edu.cn)

13
14 **Abstract.** A three-layer (Earth-air-ionosphere) physical model, as well as a
15 two-layer (Earth-air) model, is employed in this paper to investigate the ionospheric
16 effect on the wave fields for a finite length dipole current source co-located **at a**
17 **hypocenter depth and along** the main fault of an earthquake when the distance
18 **between the epicenter and an observing station** is up to one thousand kilometers or
19 even more. The results show that all electrical fields are free of ionospheric effect for
20 different frequencies in a relative short range, e.g., ~ 300 km for $f=1$ Hz, implying
21 the ionospheric influence on electromagnetic fields can be neglected within this range,
22 **which** becomes smaller as the frequency increases. However, the ionosphere can give
23 a constructive interference to the waves passed through and make them decay slowly
24 when an observation is out of this range and the ionospheric effect can be up to 1-2
25 magnitudes of the electrical fields. For an **ground-based** observable 1.3 mV m^{-1}
26 electric signal **at $f=1$ Hz** at 1,440 km away **from** the Wenchuan $M_S=8.0$ earthquake,
27 the expected seismo-telluric current magnitude for the Earth-air-ionosphere model is
28 of $5.0 \times 10^7 \text{ A}$, one magnitude smaller than the current value of $3.7 \times 10^8 \text{ A}$ obtained by
29 the Earth-air model free of ionospheric effect. This indicates that the ionosphere
30 facilitates the electromagnetic wave propagation, as if the detectability of the system
31 is improved effectively and it is easier to record a signal even for stations located at
32 distances beyond their detectability threshold. **Furthermore, the radiating patterns of**
33 **the electrical field components $|E_x|$ and $|E_y|$ are complementary each other although**
34 **anyone 2-D power distribution of them shows strong power areas as well as weak**

35 ones, which is advantageous to register a signal if the observing system is designed to
36 measure both of them instead of only one.

37

38 **Keywords.** Ionospheric influence on electromagnetic waves; The Wenchuan
39 earthquake; Seismo-telluric current; 2-D power distribution

40

41 **1 Introduction**

42 The fact that Electro-Magnetic (EM) emissions accompany every stage of large
43 earthquake preparations seems undebatable although short-term earthquake prediction
44 is still one of the most challenging targets in Earth science today (Eftaxias et al.,
45 (2002). Meanwhile, the Ultra-Low Frequency (ULF) band is of particular interest
46 because only EM signals in the ULF range and at lower frequencies originated in the
47 Earth's crust can be easily recorded at the Earth's surface without significant
48 attenuation comparing with 'high' frequency emissions that might be emitted at
49 epicenter depths at more than 10 km, even several hundreds of kilometers. Recently,
50 an increasing number of ground-based observing ULF electromagnetic emissions
51 related to strong earthquakes have been recorded at a distance of several, hundred,
52 and even several thousand kilometers. Some notable examples include the Loma
53 Prieta $M_s=7.1$ earthquake on October 17, 1989 ($f=0.01-10$ Hz, $D=7$ km, $A=1.5$ nT)
54 (Fraser-Smith et al., 1990; Bernardi et al., 1991), as well as the Spitak $M_s=6.9$
55 earthquake on December 7, 1988 ($f=0.005-1$ Hz, $D=200$ km, $A=0.2$ nT) (Molchanov
56 et al., 1992; Kopytenko et al., 1993). In addition, the geo-electric potential
57 enhancement appeared 1–19 days before five of all six EQs with magnitude >5 that
58 occurred within 75 km in Japan and its duration and intensity were several minutes to
59 1 h with an amplitude of $0.01-0.02$ mV m⁻¹ (Uyeda et al., 2000). Qian *et al.* (2002)
60 have reported the observation of ULF signals generated from Jiji earthquake of 21
61 September 1999 in Taiwan and recorded at many stations at distances of 300–900 km
62 in South East China. Similarly, Ohta *et al.* (2002) have reported the observation of
63 ULF/ELF emissions generated from Taiwan earthquake of 21 September, 1999 and
64 recorded at Nakatsugawa station in Japan at a distance of up to 2000 km.

65 A more notable example reported by Li et al. (2013) is the Wenchuan $M_s=8.0$
66 earthquake on May 12, 2008, a typical mid-crust, which resulted in great devastation
67 and 69,000 deaths. This earthquake was preceded by more than one month of
68 increasing anomalous ULF emissions with a climax starting on May 9, three days

69 before the Wenchuan main shock ($f=0.1-10$ Hz, $D=1,440$ km, $A=1.3$ mV m⁻¹).

70 Many simulating rock-pressure experiments were carried out in order to
71 understand the producing mechanism of the electromagnetic information associated
72 with seismic activities. Laboratory experiments by *Qian et al.*, [1996; 2003] and *Hao*
73 *et al.* [2003] present that, electromagnetic signals are always recorded when rock
74 samples are subjected to dynamic stresses. Electromagnetic pulses of shorter-period
75 appearing at the last stage of the experiment may be induced by instantaneous electric
76 current of the accumulated charge during the stress acceleration. The work of Freund
77 *et al.* (Freund and Wengeler, 1982, Freund, 2002, 2009, 2010; Freund and Sornette,
78 2007; Scoville *et al.*, 2015) has gained a new insight into the production of current
79 and electromagnetic signals in stressed rocks. As rocks upon stressing, stresses cause
80 slight displacements of mineral grains in the rocks, which in turn lead to the activation
81 of peroxy defects that preferentially sit on or across grain boundaries. The peroxy
82 break-up leads to positive holes h^* and the h^* are able to flow from stressed to
83 unstressed rock, traveling fast and far by way of a phonon-assisted electron hopping
84 mechanism using energy levels at the upper edge of the valence band. A gabbro
85 sample ($30 \times 15 \times 10$ cm³) from Shanxi, China, was used in the test and a 55 nA current
86 recorded about 2 seconds before failure, with the load being at about 30,000 lbs and
87 the maximum spike reaches 450 nA when the main failure took place (Freund, 2009).

88 Up to now, no clear explanation has been given although several physical
89 mechanisms have been proposed to interpret the generation of EM emissions and
90 electrical currents observed either during seismic activity or in the laboratory
91 experiments. These include the electrokinetic and magnetohydrodynamic,
92 piezomagnetism, stress-induced variations in crustal conductivity, microfracturing,
93 and so on (Draganov *et al.*, 1991; Park, 1996; Fenoglio *et al.*, 1995; Egbert, 2002;
94 Simpson and Taflove, 2005). Whatever the physical mechanism of electromagnetic
95 generation is, it is well established that, during rock experiments conducted under
96 laboratory conditions, a strong electrical current is produced when rocks are stressed,
97 especially at the stage of the main rupture.

98 As the development of satellite Earth Observation (EO), there is an increasing
99 amount of evidence that during some last stages of the long term process of
100 preparation, there could be a transfer of energy between lithosphere, atmosphere and
101 ionosphere, so as to introduce the concept of a lithosphere–atmosphere–ionosphere
102 coupling (LAIC) among the three involved layers of the Earth (Pulinets *et al.*, 1994,

103 2000; Hayakawa and Molchanov, 2002; Molchanov et al., 2004; Kamogawa, 2006).
104 When we investigate electromagnetic emissions induced by an electrical current or a
105 magnetic moment on the surface or beneath the Earth, the effect of the medium air,
106 crustal as well as ionosphere should be taken into account because of these three
107 media being of different conductivities and so we need to consider a
108 lithosphere-atmosphere-ionosphere electromagnetic coupling (Cummer, 2000).
109 Several tentative LAIC models have been constructed based on ground-based and
110 ionospheric observations prior to strong earthquakes and the investigation of influence
111 of external electrical field on ionospheric parameters has been developed quickly
112 (Pulinets and Ouzounov, 2011; Pulinets and Davidenko, 2014; Sorokin and Hayakawa,
113 2013; Sorokin and Hayakawa, 2014; Kuo et al., 2011, 2014; Namgaladze et al., 2012;
114 Zolotov et al., 2012; Zolotov, 2015). At the same time, the ionosphere plays an
115 important role in electromagnetic propagation at Extremely Low Frequency (ELF)
116 and Very Low Frequency (VLF), the ground and the ionosphere are good electrical
117 conductors and form a spherical Earth-ionosphere waveguide (Cummer, 2000). In
118 addition, in the Controlled Source Electromagnetic (CSEM) method, widely used in
119 petroleum exploration or mining, the ionospheric influence on electromagnetic (EM)
120 fields should be considered when the distance between a large-scale and large-power
121 fixed source and the receiver is up to one thousand kilometers. EM fields can be
122 amplified in the ionosphere as it is shown when we use analytical solutions of
123 Maxwell equations, as well as numerical ones of the “Earth-ionosphere” mode with a
124 source on the Earth’s surface or in the lower atmosphere (Fu et al., 2012; Li et al.,
125 2010a; Li et al., 2010b; Xu et al., 2012; Li et al., 2011).

126 Therefore, comparing with an electromagnetic attenuation without ionospheric
127 effect, the point is to evaluate the ionospheric influence on the electromagnetic
128 propagation when the distance between the epicenter and the observing location is up
129 to one thousand kilometers or even more. Furthermore, the comparison between the
130 observation distance reported by Li et al. (2013) ($D=1,440$ km) and the length of the
131 Wenchuan earthquake main rupture $L \sim 150$ km (Zhang et al., 2009) indicates that
132 the length of the dipole source is not negligible. So in this paper, based on the work of
133 Key (2009), a three-layer (Earth-air-ionosphere) physical model, as well as a
134 two-layer (Earth-air) model, containing a finite length dipole current source
135 co-located along the fault and beneath the Earth is introduced in Sect. 2. For specified
136 parameters, some simulation results of the current source with and without

137 ionospheric effect are given in Sect. 3. In Sect.4, using assumed parameters, the
 138 simulation results for the case of the Wenchuan earthquake reported by Li et al. (2013)
 139 are presented. Discussion and conclusions are given in Sect. 5 and Sect.6,
 140 respectively.

141

142 2 Description of the modeling methodology

143 In order to study the electromagnetic fields emitted by a long dipole current
 144 source, the approach used here follows the magnetic vector potential formulation
 145 described in Wait (1982) and developed by Key (2009), who generalized the
 146 formulation to allow for multiple layers above the transmitter (in addition to multiple
 147 layers below). He used exponential forms for the recursions rather than hyperbolic
 148 functions in isotropic media, which consists of N layers of isotropic conductivity σ_i
 149 where $i = 1, \dots, N$, and which uses a right-handed coordinate system with the z axis
 150 pointing down. Assuming a time-harmonic source with $e^{-i\omega t}$ time dependence,
 151 negligible magnetic permeability μ variations, and angular frequencies ω that are
 152 low enough so that displacement currents can be neglected, Maxwell's equations are

$$153 \quad \nabla \times \mathbf{E} = i\omega\mathbf{B}, \quad (1)$$

154 and

$$155 \quad \nabla \times \mathbf{B} = \mu\sigma\mathbf{E} + \mu\mathbf{J}_s. \quad (2)$$

156 Expression $\mathbf{J}_s = \mathbf{I}\delta(\mathbf{r} - \mathbf{r}_0)$ is the imposed electric dipole source at position \mathbf{r}_0 with
 157 vector moment \mathbf{I} , and here is restricted to an infinitesimal dipole with unit moment.

158

159

160

161

162

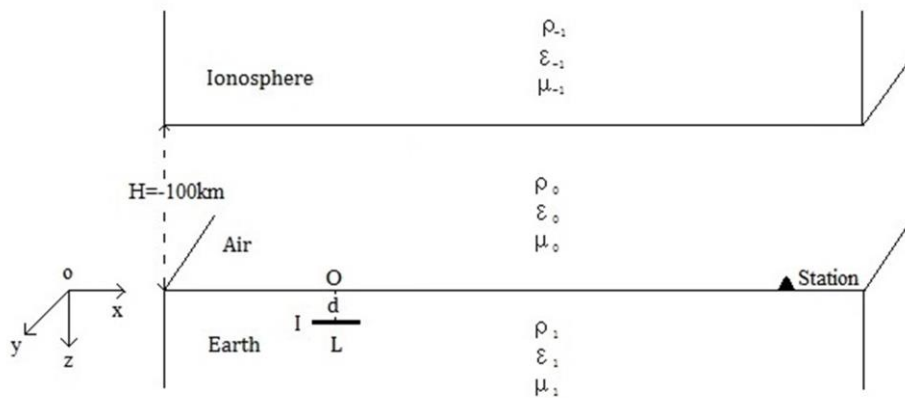
163

164

165

166

167



168 **Fig.1.** An x-directed dipole current source, with its central coordinate (0, 0, d), is placed in the
 169 bottom medium (Earth) of a three layer modeling (Earth-air-ionosphere model), where z is defined
 170 positive in the downward direction.

171 Based on the model set up by Key (2009), some modifications will be done in
172 this study in order to answer the questions illustrated above. A physical model is
173 specified. It has three layers, Earth, air and ionosphere, which is called
174 Earth-air-ionosphere model. Its coordinate system is denoted in Fig.1 **with z-direction**
175 **being downward**. An x-directed dipole of a length L and a current I is placed in the
176 bottom medium (Earth: $z > 0$), which is homogeneous and has the electrical
177 properties: magnetic permeability μ_1 , permittivity ϵ_1 , and conductivity σ_1 . The
178 middle medium (air: $-100 \text{ km} < z < 0$) is described by its electrical properties μ_0 ,
179 $\epsilon_0 (= 8.854 \times 10^{-12} \text{ Farad m}^{-1})$ and $\sigma_0 (= 10^{-14} \text{ S m}^{-1})$. The top medium
180 (ionosphere: $z < -100 \text{ km}$) is characterized by electrical properties μ_{-1} , ϵ_{-1} and
181 $\sigma_{-1} (= 10^{-5} \text{ S m}^{-1})$.

182 As a comparison, a two-layer model (Earth-air model) including in Earth
183 medium ($z > 0$), as well as air medium ($z < 0$), is also established during the study.
184 All the corresponding parameters described are the same as these of
185 Earth-air-ionosphere model.

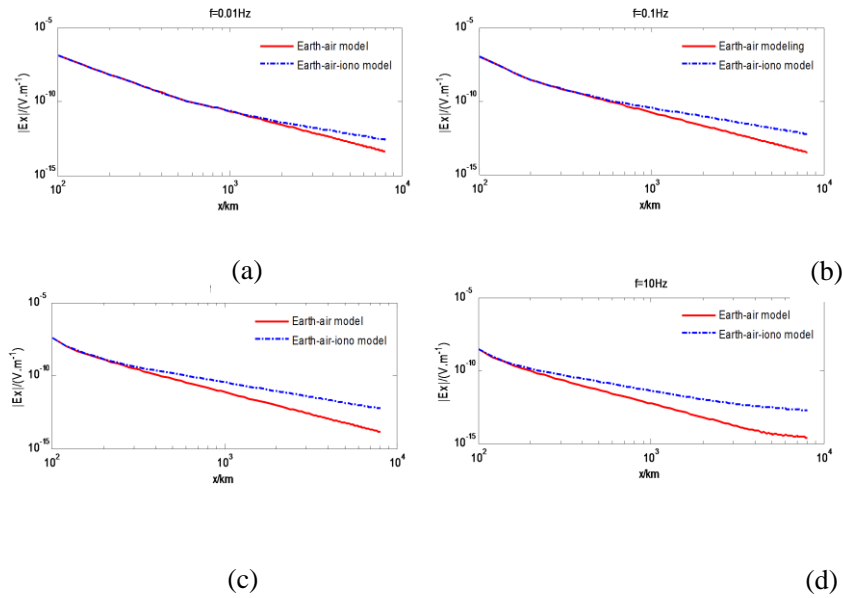
186 We assume that the total space is non-magnetic and that the magnetic
187 permeability variations are negligible in the different layers, i.e. $\mu_1 = \mu_0 = \mu_{-1} =$
188 $4\pi \times 10^{-7} \text{ Farad m}^{-1}$. However, the ionosphere as the electrically conducting
189 section of the upper atmosphere plays **such an** important role **for** the electromagnetic
190 propagation that we set $\epsilon_{-1} = 5\epsilon_0$ when an ionospheric effect on electromagnetic
191 transmission is taken into consideration. On the same manner we have $\epsilon_1 = \epsilon_0 =$
192 $8.854 \times 10^{-12} \text{ Farad m}^{-1}$, i.e. ϵ_1 is not considered as zero during all calculations.
193 Under these conditions, the formula listed above are still suitable and more
194 explanations about the potential formulation of a horizontal electric dipole can be
195 found in the Appendix A of Key (2009) and related programs are available with an
196 access to the website (<http://marineemlab.ucsd.edu/>). The horizontal finite length
197 dipole source can be **viewed** as integral of an infinite small horizontal dipole during
198 related calculations.

199

200 **3 Simulation results**

201 According to these two models **presented** above, several free parameters must be
202 specified in order to investigate the attenuation characteristics of the electromagnetic
203 fields emitted by a long x-directed dipole current source. As for the parameters of the
204 dipole current source, we select $L=150 \text{ km}$, the Wenchuan earthquake main rupture

205 stage within 30 s out of 90 s (~ 300 km) based on Zhang et al., (2009, Fig.1), the
 206 depth $d = 19$ km (Xu, 2009), the hypocenter depth of the Wenchuan case and the
 207 current is set to be $I = 1$ A temporarily. Here, the Earth is considered to be an isotropic
 208 media with an average conductivity σ_1 , and we assume $\sigma_1 = 1.0 \times 10^{-3} \text{ S m}^{-1}$ at
 209 this time, i.e. $\rho_1 = 10^3 \text{ ohm} \cdot \text{m}$, although the ground conductivity depends not only
 210 on the local petrology, but also on the porosity, temperature, and pressure (e.g., Wait,
 211 1966). All these parameters are common to two models. The parameter $\epsilon_{-1} = 5\epsilon_0$ is
 212 of most importance during the calculation in three-layer model in that it can
 213 potentially affect the transmission of electromagnetic waves produced by the dipole
 214 beneath the Earth, and possibly induce the Earth-atmosphere-ionosphere
 215 electromagnetic coupling.



230 **Fig.2.** Electric field $|E_x|$ decay curves along x-axis direction as a function of the observing
 231 distance for the Cartesian coordinate system with different frequencies. Red solid lines stand for
 232 electric field curves for Earth-air model and blue dot lines denote electric field curves with the
 233 ionospheric effect for Earth-air-ionosphere model.

- 234 (a) Total $|E_x|$ for $f = 0.01$ Hz; (b) Total $|E_x|$ for $f = 0.1$ Hz;
 235 (c) Total $|E_x|$ for $f = 1$ Hz; (d) Total $|E_x|$ for $f = 10$ Hz;

239 Fig.2a-d displays electric field amplitude $|E_x|$ decay curves along the x-axial
240 direction with the frequencies $f=0.01$ Hz, $f=0.1$ Hz, $f=1$ Hz, and $f=10$ Hz respectively
241 for the Cartesian coordinate system up to $\sim 10,000$ km on the Earth's surface.

242 It can be seen from Fig.2a-d, first, the electrical field with "high" frequency has a
243 big attenuation although all curves for both Earth-air model (red solid lines) and
244 Earth-air-ionosphere model (blue dot lines) decay rapidly as the distance increases.
245 Second, each group of curves run at the same level for one fixed frequency, e.g., $f=1$
246 Hz, when an observing point is located at a relative near distance, ~ 300 km for $f=1$
247 Hz (Fig.2c) for example. That is to say, the ionospheric influence on electromagnetic
248 field transmissions can be neglected within this range. However this range changes
249 for different frequencies and it becomes smaller as the operating frequency of the
250 current source increases (e.g., more than 1000 km for $f=0.01$ Hz (Fig.2a) and only
251 ~ 200 km for $f=10$ Hz (Fig.2d)). Third, the most important result is, as the distance
252 increases, field curves with an ionospheric effect (blue dot lines) run **along** a different
253 **path** from that of curves without an ionospheric effect (red solid lines) and the
254 ionospheric lines attenuate more slowly. Now, this kind of ionospheric influence can
255 no longer be neglected. The ionospheric difference is about 1 magnitude ($\times 10$) for all
256 the frequencies listed and even once up to 2 magnitudes for $f=10$ Hz within the range
257 shown in Fig.2. For example, the ionospheric difference value shows 1 magnitude
258 from ~ 840 km, up to 2 magnitudes from $\sim 3,700$ km for $f=10$ Hz (Fig.2d).

259

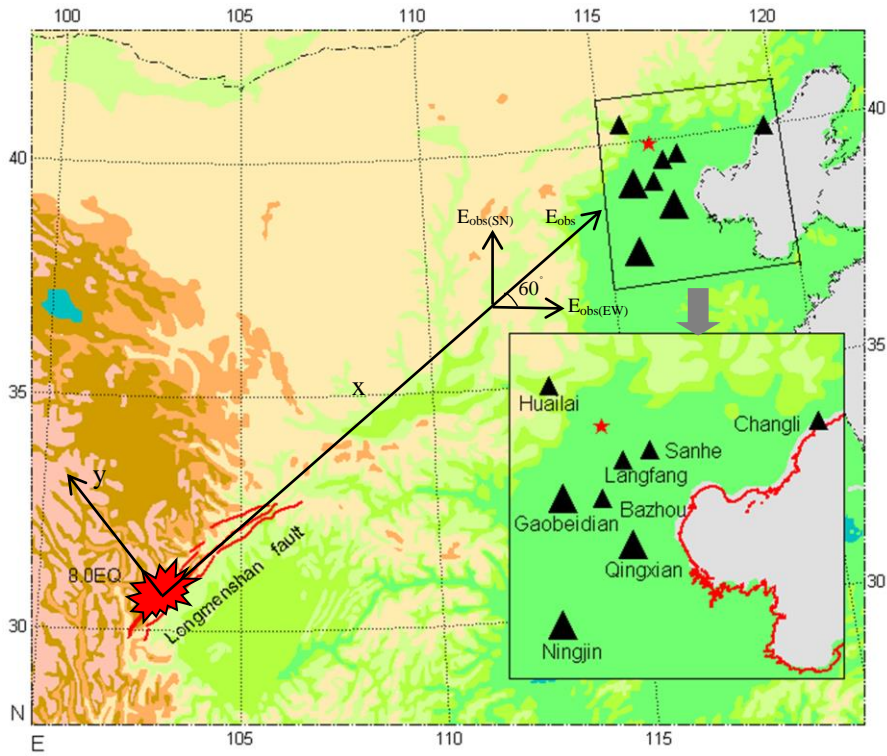
260 **4 The Wenchuan $M_S=8.0$ earthquake as a sample**

261 **4.1 Estimating the seismo-telluric current magnitude**

262 On the base of the work of rock experiments conducted under laboratory
263 conditions, there is a reason to believe that a giant seismo-telluric current is generated
264 when the main rupture took place during the Wenchuan earthquake on 12 May 2008
265 and that this current mainly **propagated** along the Longmenshan fault. At the same
266 time a strong electrical field induced by this current suddenly increased. This
267 electrical field was recorded at the ground-based Gaobeidian ULF observing station,
268 1440 km away from the epicenter of the shock, with a SN (**South-North**) maximum
269 amplitude of 70 mm, i.e. 1.3 mV m^{-1} (Li et al., 2013), that is $E_{\text{obs(SN)}} = 1.3 \text{ mV m}^{-1}$ in
270 the following statement (Fig. 3).

271

272
 273
 274
 275
 276
 277
 278
 279
 280
 281
 282
 283
 284
 285
 286
 287



288 **Fig.3.** Distribution of the Wenchuan earthquake epicenter and observation stations. Black solid
 289 triangles present the related locations of observation stations in Hebei electromagnetic observation
 290 network, bigger ones indicate the stations where abnormal information was recorded and the red
 291 star denotes Beijing (Li et al., 2013, Fig.1). A ground surface coordinate system is added.
 292

293 In order to establish a relationship between the seismo-telluric current during the
 294 main event and the observable ground electrical signals registered at Gaobeidian
 295 station, we consider that a finite length current dipole source, with the length being
 296 the main rupture $L=150$ km of the Wenchuan earthquake and the current I , is
 297 co-located with the Longmenshan main fault (x-direction), with the depth being $d=19$
 298 km. Then one can refer to Fig.1 with ionospheric effect.

299 **Corresponding to Fig.1,** a coordinate system on the Earth's surface (see Fig.3) is
 300 set up to calculate the observable electrical field along the x-direction E_{obs} according
 301 to the electrical value $E_{obs(SN)}=1.3$ mV m⁻¹ recorded at the Gaobeidian station. The
 302 Gaobeidian station lies in the extended line of the Longmenshan fault, which trends
 303 northeast and dips about 60° west (Xu, 2009). Other locations of stations are shown in
 304 Fig.1 of Li et al. (2013) and here they are shown in Fig.3 which includes a ground
 305 surface coordinate system. From Fig.3, we see that the electrical field component

306 intensity along the x-direction is about $|E_x|=E_{\text{obs}}=1.5 \text{ mV m}^{-1}$ ($E_{\text{obs(SN)}}=\sin 60^\circ \times$
 307 $E_{\text{obs}}=1.3 \text{ mV m}^{-1} \rightarrow E_{\text{obs}}=1.5 \text{ mV m}^{-1}$).

308 As the observing frequency of the electromagnetic observation system is 0.1-10
 309 Hz and the recorder belongs to a real-time analog record, it is not easy to figure out
 310 the right frequency of the signals registered at the Gaobeidian station during the
 311 maximum stage prior to the Wenchuan earthquake. We set the main frequency $f=1$ Hz
 312 during our calculations although the information is of a short period $\sim 0.1-0.3$ s and a
 313 large amplitude $\sim 1.3 \text{ mV m}^{-1}$ (Li et al., 2013) and frequency bands (0.4-3 s and
 314 0.05-0.1 s) with various amplitudes were observed (Guan et al., 2003). At the same
 315 time, the results of 2D MT inversion in the Longmenshan fault show that the apparent
 316 resistivity logarithm is $\sim 1-4.8$ (Zhu et al., 2008) and it is a wide range.

317

318

319

320

321

322

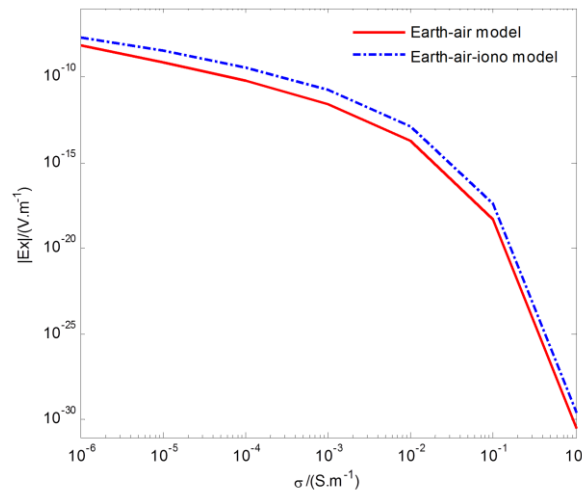
323

324

325

326

327



328 **Fig.4.** The calculated value of $|E_x|$, expected at the observation location (1,440 km, 0, 0) due to a
 329 dipole source of $L=150$ km, $I=1$ A, $f=1$ Hz and $d=19$ km (Fig.1), as a function of the typical
 330 crustal materials conductivity σ both in Earth-air model (red line) and in Earth-air-ionosphere
 331 model (blue dot line).

332

333 Fig. 4 shows the calculated values of $|E_x|$, expected at the observation location
 334 (1,440 km, 0, 0) due to a dipole source of $L=150$ km, $I=1$ A and $d=19$ km (Fig.1), as a
 335 function of the typical crustal materials conductivity σ . Comparing with the red line
 336 with the blue dot one, the ionospheric effect is clearly displayed throughout the
 337 variation of the crustal conductivity. A rapid attenuation (in excess of 20 of magnitude)
 338 of the field values indicates the importance of the conductivity σ . It is difficult to
 339 specify the average conductivity σ (referred to as σ_1 in the context) of the

340 homogeneous Earth medium, even for the typical Wenchuan area. However,
341 combined with $f=1$ Hz here, the skin-depth depends on the conductivity σ , given by
342 the formula $\delta = (\pi f \mu_0 \sigma)^{-\frac{1}{2}}$. Taken the depth $d=19$ km into account, here $\delta = d =$
343 19 km and the calculated σ_1 is attained, i.e. $\sigma_1 = 7.0 \times 10^{-4} \text{ S m}^{-1}$, which is
344 advantageous to radiate electromagnetic waves within this depth.

345 Using the same parameters as above, the simulation results show that the
346 seismo-telluric current along the main fault needed to produce an electrical ground
347 signal $E_{\text{obs(SN)}} = 1.3 \text{ mV m}^{-1}$ at the Gaobeidian station when the Wenchuan event
348 occurred, is about $5.0 \times 10^7 \text{ A}$ with the ionospheric effect and $3.7 \times 10^8 \text{ A}$ without the
349 ionospheric effect. As it is expected, these two results have one magnitude ($\times 10$)
350 difference from each other. While the former is more reasonable under this conditions
351 because the seismo-telluric current produced by the Wenchuan main rupture is
352 specified.

353

354 **4.2. Detectability under the ionospheric effect**

355 Now according to the Wenchuan earthquake example, the seismo-telluric current
356 source ($f=1$ Hz, $d =19$ km, $L=150$ km, and a current $I=5.0 \times 10^7 \text{ A}$ considering the
357 Earth-air-ionosphere model) is thought of as a powerful finite length dipole source.

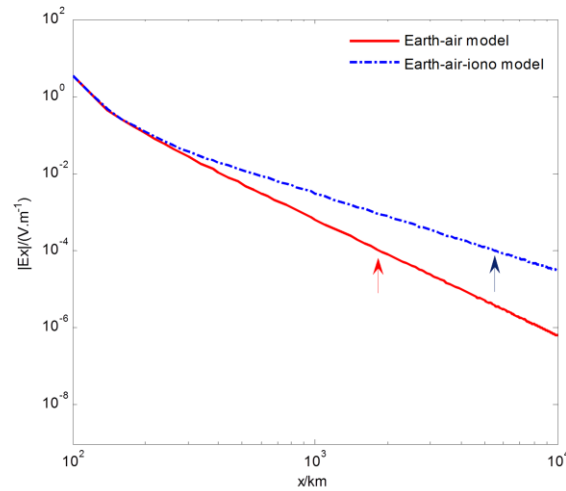
358 Fig.5 displays the fluctuations of the surface electrical fields with and without
359 ionospheric effect for the Wenchuan source along x-axial direction. It shows no
360 obvious ionospheric effect within 300 km, while this effect is roughly up to 1 **order of**
361 magnitude from ~ 800 km. The gap becomes larger as the distance **increases**, near 2
362 magnitudes from ~ 9000 km, and then it keeps this gap till 10,000 km. Under this
363 condition, **if the resolution of an observing system is 0.1 mV m^{-1} , the distance**
364 **recorded such a signal must be ~ 5400 km (blue arrow) with ionospheric effect, or it is**
365 **only ~ 1800 km (red arrow) without ionospheric effect.** So the ionosphere facilitates
366 the electromagnetic wave propagation, as if the detectability of the system **were**
367 improved effectively and it **would be** easier to record a signal even **at** stations located
368 beyond their detectability threshold.

369

370

371

372
373
374
375
376
377
378
379
380
381
382
383



384 **Fig.5.** The Wenchuan source producing electric field $|E_x|$ decay curves as a function of the
385 distance along x-axial direction with ionospheric effect (blue dot line), as well as without
386 ionospheric effect (red line). The electric field $|E_x|=0.1 \text{ mV m}^{-1}$ is labeled by a red arrow and a
387 blue one respectively.

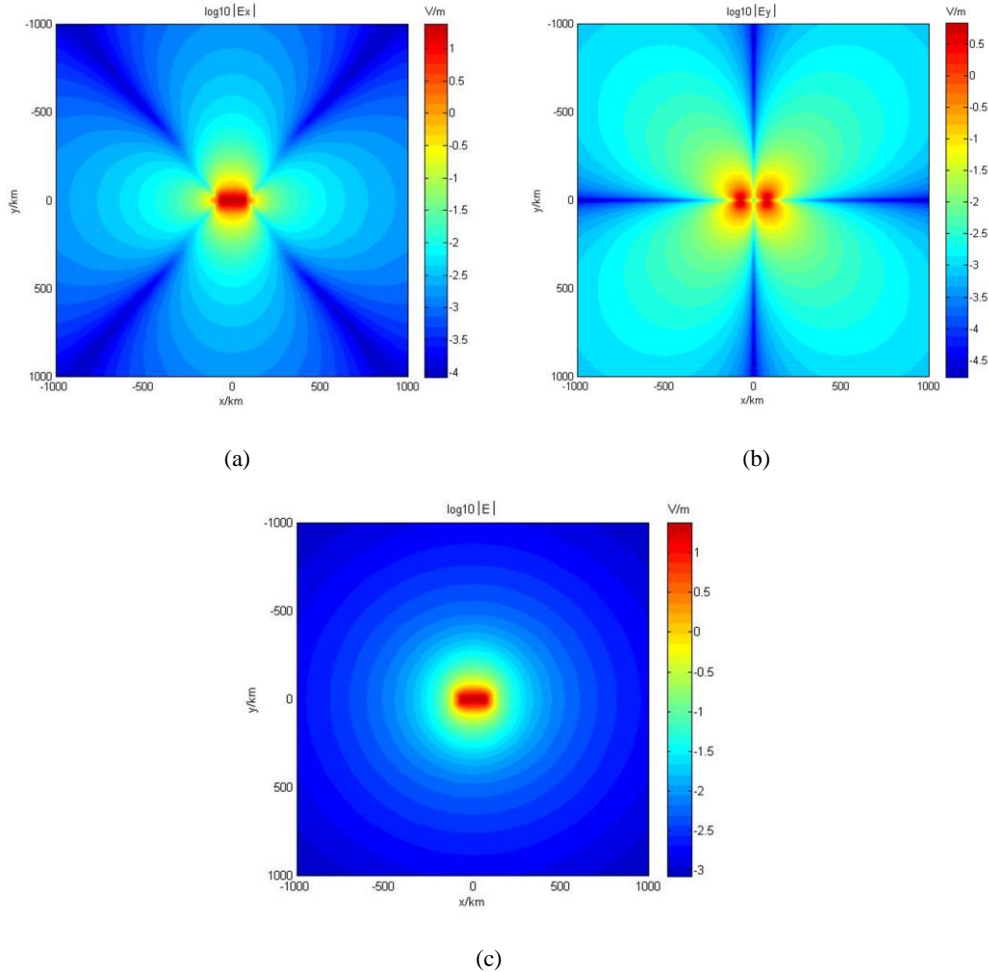
388
389

4.3. Wave 2-D distribution

390 We perform electromagnetic wave fields for the Wenchuan source and this is
391 done in the ground plane region $-1,000 \text{ km} < x < 1,000 \text{ km}$ and $-1,000 \text{ km} < y < 1,000 \text{ km}$
392 in order to visualize the 2-D distribution of the wave power surrounding the electrical
393 source.

394 Figure 6 displays the 2-D power distributions of the electrical field components
395 $|E_x|$, $|E_y|$ and the total $|E|$ ($|E|^2 = |E_x|^2 + |E_y|^2$) after making a logarithm calculation on
396 the Earth's surface. It can be seen firstly from Figure 6a that there is an obvious
397 constant strong power along the current element length ($-75 \text{ km} < x < 75 \text{ km}$) in the
398 x-direction. The electrical value in this area is not discussed here because it is usually
399 considered not precise. Then the strong field radiates outward surrounding four main
400 axes, indicating 1 order rough decay of the field at $\sim 160 \text{ km}$, 2 orders of magnitude
401 at $\sim 320 \text{ km}$ from the source endpoint in the x-direction. There is only 3 orders decay
402 till 1,000 km away because of the ionospheric facilitating effect on the field and it
403 keeps a strong value ($\sim 1.86 \text{ mV}$) which can be fairly recorded by the stations.
404 However, there are also weak power areas along lines, which form 45° angle with the
405 principal axis for the electrical field power $|E_x|$ (Figure 6a). Complementally, the
406 electrical field power $|E_y|$ (Figure 6b) is basically characterized by strong power areas

407 between two main axes, as well as weak ones along four chief axes. The power
 408 distribution of the total $|E|$ consequently presents to be symmetry to the center circle
 409 outside of the source (Figure 6c), which also indicates that the radiating patterns of
 410 the electrical field power $|E_x|$ and the electrical field power $|E_y|$ are complementary
 411 (One is strong area and the other is weak area) each other surrounding the source.



437 **Fig.6.** 2-D distributions of electrical field power $|E_x|$ (a), $|E_y|$ (b) and total $|E|$ (c) after a
 438 logarithm calculation for the Wenchuan source using Earth-air-ionosphere model.

440 5 Discussion

441 In very recent years, there is an increasing amount of evidence that during some
 442 last stages of the long term process of preparation, there could be a transfer of energy
 443 between lithosphere and the above layers of atmosphere and ionosphere, so as to
 444 introduce the concept of a lithosphere–atmosphere–ionosphere coupling (LAIC)
 445 among the three involved layers of the Earth system (Pulinets et al., 2000; Hayakawa
 446 and Molchanov, 2002; Molchanov et al., 2004; Pulinets and Ouzounov, 2011). On

447 one hand, the ‘energy source’ is usually thought to be beneath the Earth’s surface and
448 related to tectonic activities in the lithosphere. On the other hand, numerous
449 rock-pressure experiments and electromagnetic observations associated with seismic
450 activities have already proved that a giant electrical current and an abrupt increase of
451 electromagnetic signals occur during the main rupture of stressed-rocks. These
452 phenomena happened on May 9 2008, 3 days before the Wenchuan event, which
453 hypocenter lies in mid-crust. The strong seismo-telluric current is thought to run
454 mainly along the Longmenshan fault and electromagnetic oscillations, induced by the
455 current and predominated by ULF frequency band, propagate up to ionosphere and
456 give rise to perturbations of ionospheric parameters. Some of these parameters have
457 been investigated, such as GPS TEC and f₀F₂ (Yu et al., 2009; Xu et al., 2010;
458 Akhoondzadeh et al., 2010), DEMETER satellite O⁺ density (Zhang et al., 2009),
459 electron density and electron temperature (Zeng et al., 2009), and so on. Fortunately,
460 all these study results present a climax on May 9 and this indicates a lithosphere–
461 atmosphere–ionosphere coupling or interaction aroused by these electromagnetic
462 signals prior to the Wenchuan event.

463 Unfortunately, at present, most of investigations put emphases on the effect of
464 earthquakes upon the ionosphere and few of them pay attention to an inverse problem,
465 that is the ionospheric influence on the electromagnetic waves passing through.

466 The ionosphere, as a part of the electrical conducting region of the upper
467 atmosphere, can enhance electromagnetic fields and cause the decay as a function of
468 distance to slow down when an observation is within ionospheric range and the
469 ionospheric effect can be up to 1-2 magnitudes of the electrical fields in our simply
470 three-layer model for some specified parameters we have selected here.

471 Considering the Wenchuan event, the electrical signals from the lithosphere
472 interact with the ionosphere and are at the same time enhanced, and then registered at
473 1440 km Gaobeidian station with the amplitude of 1.3 mV m⁻¹. This electrical field is
474 used to simulate the seismo-telluric current produced by the Wenchuan main rupture
475 in an Earth-air-ionosphere model together with an Earth-air model. The results present
476 that, the seismo-telluric currents with and without ionospheric effect must be about
477 5.0×10^7 A and 3.7×10^8 A respectively. Compared with the expected seismo-telluric
478 current ~10–100 kA of the “Alum Rock” $M_w=5.6$ earthquake for an observed 30 nT
479 pulse at 1 Hz and D=2 km (Bortnik et al., 2010), this result is probably in a reasonable
480 range.

481 However, firstly, the total rupture of the Longmenshan fault during the
482 Wenchuan main shock is extremely complicated that comprises of tenths of rupture
483 stages and several pauses, totaling 90 s for the whole rupture process (~ 300 km),
484 according to Zhang et al.,(2009). Thus the total surface rupture ~ 300 km is
485 nevertheless not used here. While performing the analysis on only the primary 30 s, a
486 main stage of the Wenchuan earthquake, out of 90 s as we have selected $L=150$ km
487 above, is expected to be representative of the majority of the rupture to generate a
488 seismo-telluric current. Secondly, three medium are thought of as a homogeneous
489 isotropic medium in our models and with the same average conductivity value for
490 each one, especially for the wenchuan area. However, the Earth conductivity plays
491 such an important role that it predominately affects the fluctuations of the electrical
492 fields as shown in Fig.4 although no one exactly knows the right conductivity of the
493 Earth medium at the rupture depth. The value $\sigma_1 = 7.0 \times 10^{-4} \text{ S m}^{-1}$ taken part in
494 all analysis is estimated when the observing frequency range $f=0.1-10$ Hz and the
495 hypocenter depth $d=19$ km of the Wenchuan main event are taken into account for the
496 skin-depth formula. One must also mention that we use $f=1$ Hz in our calculations
497 because we cannot identify the actual frequencies in the recorded analog signals. All
498 these can probably underscore our simulation results.

499 While these disadvantageous selections maybe are not so important at the same
500 time because the key point of this paper is of the ionospheric influence on
501 electromagnetic wave propagation and our investigation attains advantageous results.

502 The “selectivity” or “orientation” of the electromagnetic information is a very
503 important character during seismic activities (Varotsos and Lazaridou, 1991). For a
504 finite length dipole source of the Wenchuan earthquake, its 2-D distributions of
505 electrical field component $|E_x|$ and $|E_y|$, which are orthogonal each other, on the
506 Earth’s surface shows there are strong field power areas and weak field power areas
507 around the source as illustrated by [Bortnik et al., 2010]. While the radiating pattern
508 of the total $|E|$ in this investigation is symmetry to the center circle outside of the
509 source which indicates a signal is always registered to anyone direction if a system is
510 designed to measure the total field $|E|$ or both of $|E_x|$ and $|E_y|$ components instead of
511 only one. This result also basically supports the practices of “selectivity” or
512 “orientation”, the observing reality before the Wenchuan earthquake described by Li
513 et al.[2013], for example, ‘Compared with the EW (East-West) orientation, the
514 electromagnetic signal is more obvious in the SN (South-North) orientation’. The

515 selectivity effect is a complex phenomenon that may be attributed to a superposition
516 of the following three factors: “source characteristics”, “travel path” and
517 “inhomogeneities close to the station” [Varotsos and Lazaridou, 1991; Varotsos et al.,
518 2005]. Analytical solutions of Maxwell equations [Varotsos et al., 2000], as well as
519 numerical ones [Sarlis et al., 1999], convince that selectivity results from the fact that
520 earthquakes occur by slip on faults which are appreciably more conductive than the
521 surrounding medium.

522

523 **6 Conclusions**

524 In this paper, a three-layer (Earth-air-ionosphere) physical model, as well as a
525 two-layer (Earth-air) model, is employed to investigate the ionospheric effect on the
526 wave fields for a finite length dipole current source co-located with the main fault of
527 an earthquake when an observing location distance is up to one thousand kilometers
528 or even more. For a dipole source with specified parameters of the length $L=150$ km,
529 the current $I=1$ A, and the depth $d=19$ km, the results show that all fields are free of
530 the ionospheric effect for different frequencies in relative short ranges, e.g., ~ 600
531 km for $f=0.1$ Hz, which implies the ionospheric influence on electromagnetic field
532 transmissions can be neglected within this range. However, the ionosphere can
533 increase the field amplitude and slow the decay when an observation is out of this
534 range and the ionospheric effect can be up to 1-2 magnitudes of the electrical fields.

535 This is applicable to the 12 May 2008 Wenchuan $M_S=8.0$ earthquake during
536 which a strong electromagnetic signal with an amplitude of ~ 1.3 mV m⁻¹, is recorded
537 by the Gaobeidian ULF ($f=0.1-10$ Hz) observing station 1440 km from the epicenter.
538 The main fault rupture producing a current is equivalent to a finite length dipole
539 current source, with a nucleation depth of 19 km and a length of 150 km. Considering
540 the Earth-air-ionosphere model, the expected current for the most typical properties of
541 Wenchuan area is of 5.0×10^7 A, which is of one magnitude smaller than the current
542 value of 3.7×10^8 A obtained with the Earth-air model free of ionospheric effect. On
543 the contrary, a signal produced by a seismic activity can be advantageously recorded
544 by a remote station under the ionospheric effect as if the detectability of the system is
545 improved effectively.

546 The 2-D power distributions of the electrical field component $|E_x|$, $|E_y|$ and the
547 total $|E|$ after making a logarithm calculation on the Earth's surface are characterized
548 by different radiating patterns. There are strong power areas along four main axes as

549 well as weak power areas between two main axes for the electrical field $|E_x|$. While
550 the component $|E_y|$ displays a complementary radiating pattern with strong areas and
551 weak areas. Therefore, fortunately, a signal is always registered to anyone direction if
552 a system is designed to measure the total field $|E|$ (or both $|E_x|$ and $|E_y|$ components)
553 as the radiating pattern of which is Symmetry to the center circle outside of the
554 source.

555

556 *Acknowledgements and data.* The authors are grateful to the National Natural Science
557 Foundation of China and this work was sponsored by the project Simulation and
558 Interpretation of the Spatial Electromagnetic Phenomena Coupling before the
559 Wenchuan $M_S8.0$ Earthquake under grant agreement n^o41204057. The data presented
560 in this paper are available to the e-mail: limeixuxl@seis.ac.cn.

561

562 Edited by: C. Krawczyk

563 Reviewed by: F. Freund and one anonymous reviewer

564

565 **References**

- 566 Akhoondzadeh, M., Parrot, M., and Saradjian M. R.: Electron and ion density
567 variations before strong earthquakes ($M>6.0$) using DEMETER and GPS data, Nat.
568 Hazards Earth Syst. Sci., 10, 7–18, 2010.
- 569 Bernardi, A., Fraser-Smith, A. C., McGill, P. R., and Villard Jr, O. G.: Magnetic field
570 measurements near the epicenter of the $M_S7.1$ Loma Prieta earthquake, Phys. Earth
571 Planet, Interiors, 68, 45–63, 1991.
- 572 Bortnik, J., Bleier, T. E., Dunson, C., and Freund, F., Estimating the seismo-telluric
573 current required for observable electromagnetic ground signals, Ann. Geophys., 28,
574 1615–1624, doi:10.5194/angeo-28-1615-2010, 2010.
- 575 Cummer, S.A.: Modeling Electromagnetic Propagation in the Earth-Ionosphere
576 Waveguide, IEEE Transactions on Antennas and Propagation, 48(9), 2–12, 2000.
- 577 Draganov, A. B., Inan, U. S., and Taranenkov, Y. N.: ULF magnetic signatures at the
578 Earth due to groundwater flow: a possible precursor to earthquakes, Geophys. Res.
579 Lett., 18, 1127–1130, 1991.
- 580 Eftaxias, K., Kapiris, P., Polygiannakis, J., Peratzakis, A., Kopanas, J., Antonopoulos,
581 G., and Rigas D.: Experience of short-term earthquake precursors with VLF-VHF
582 electromagnetic emissions, Nat. Hazards Earth Syst. Sci., 3, 217–228, 2002.
- 583 Egbert, G. D.: On the generation of ULF magnetic variations by conductivity
584 fluctuations in a fault zone, Pure Appl. Geophys., 159, 1205–1227, 2002.

585 Fenoglio, M. A., Johnston, M. J. S., and Byerlee J. D.: Magnetic and electric fields
586 associated with changes in high pore pressure in fault zones: application to the
587 Loma Prieta ULF emissions, *J. Geophys. Res.*, 100 (12), 951–958, 1995.

588 Fraser-Smith, A. C., Bernardi, A., McGill, P. R., Ladd, M. E., Helliwell, R. A., and
589 Villard Jr, O. G.: Low-frequency magnetic measurements near the epicenter of the
590 *Ms* 7.1 Loma Prieta earthquake, *Geophys. Res. Lett.*, 17, 1465–1468, 1990.

591 Freund, F., and Sornette, D.: Electro-magnetic earthquake bursts and critical rupture
592 of peroxy bond networks in rocks, *Tectonophysics*, 431, 33–47, 2007.

593 Freund, F., and Wengeler, H.: The infrared spectrum of OH⁻ compensated defect sites
594 in C-doped MgO and CaO single crystals. *J. Phys. Chem. Solids* 43, 129–145,
595 1982.

596 Freund, F.: Charge generation and propagation in igneous rocks, *J. Geodynamics*, 33,
597 543–570, 2002.

598 Freund, F.: Conversion of dissolved “water” into molecular hydrogen and peroxy
599 linkages. *J. Non-Cryst. Solids* 71, 195–202, 1985.

600 Freund, F.: Stress-activated positive hole charge carriers in rocks and the generation
601 of pre-earthquake signals, in: *Electromagnetic Phenomena Associated with*
602 *Earthquakes*, edited by: Hayakawa, M., Transworld Research Network, Trivandrum,
603 India, Chapter 3, 41–96, 2009.

604 Freund, F.: Toward a unified solid state theory for pre-earthquake signals, *Acta*
605 *Geophys.*, 58(5), 719–766, 2010.

606 Fu, C. M., Di, Q. Y., Xu, C., and Wang, M. Y.: Electromagnetic fields for different
607 type sources with effect of the ionosphere, *Chinese J. Geophys.*, 55(12), 3958–3968,
608 doi: 10. 6038/ j. issn. 0001-5733. 2012. 12. 008, 2012(in Chinese with English
609 abstract).

610 Guan, H. P., Han, F.Y., Xiao, W. J., and Chen, Z.Y.: ULF electromagnetic
611 observation and data processing methods, *Earthquake*, 23(2), 5–93, 2003(in
612 Chinese with English abstract).

613 Hayakawa, M., and Molchanov, O. A. (Eds.): *Seismo-Electromagnetics:*
614 *Lithosphere-Atmosphere-Ionosphere Coupling*, Tokyo, Japan: TERRAPUB, 2002.

615 Kamogawa, M.: Pre-seismic lithosphere–atmosphere–ionosphere coupling. *Eos*
616 87(40), 2006.

617 Key, K.: 1D inversion of multicomponent, multi-frequency marine CSEM data:
618 Methodology and synthetic studies for resolving thin resistive layers, *Geophysics*,
619 74(2), F9–F20, 2009.

620 Kopytenko, Y. A., Matiashvili, T. G., Voronov, P. M., Kopytenko, E. A., and
621 Molchanov, O. A.: Detection of ultra-low frequency emissions connected with the
622 Spitak earthquake and its aftershock activity, based on geomagnetic pulsations data
623 at Dusheti and Vardzia observatories, *Phys. Earth Planet. Interiors*, 77, 85–95,

624 1993.

625 Kuo, C. L., Huba, J. D., Joyce, G., and Lee, L. C.: Ionosphere plasma bubbles and
626 density variations induced by pre-earthquake rock currents and associated surface
627 charges. *J. Geophys. Res.*, 116, A10317, 2011.

628 Kuo, C. L., Lee, L. C., and Huba, J. D.: An improved coupling model for the
629 lithosphere-atmosphere-ionosphere system, *J. Geophys. Res. Space Physics*, 119(4),
630 3189–3205, 2014.

631 Li, M., Lu, J., Parrot, M., Tan, H., and Zhang, X.: Review of unprecedented ULF
632 electromagnetic anomalous emissions possibly related to the Wenchuan $M_S = 8.0$
633 earthquake, on 12 May 2008. *Nat. Hazards Earth Syst. Sci.*, 13(2), 279–286,
634 doi: 10.5194/nhess-13-279-2013, 2013.

635 Li, D., Di, Q. Y., and Wang, M. Y.: One-dimensional electromagnetic fields forward
636 modeling for “earth–ionosphere” mode. *Chinese J. Geophys.*, 54(9), 2375–2388,
637 doi: 10.3969/j.issn.0001-5733.2011.09.021, 2011 (in Chinese with English
638 abstract).

639 Li, Y., Lin, P. R., Zheng, C. J., Shi, F. S., Xu, B. L., and Guo, P.: The electromagnetic
640 response modeling of the ELF method and the influence of the ionosphere,
641 *Geophysical & Geochemical Exploration*, 34(3), 332–339, 2010a, (in Chinese with
642 English abstract).

643 Li, D. Q., Di, Q. Y., and Wang, M. Y.: Study of large scale large power control source
644 electromagnetic with “Earth–ionosphere” mode, *Chinese J. Geophys.*, 53(2), 411–
645 420, doi: 10.3969/j.issn.0001-5733.2010.02.019, 2010b, (in Chinese with
646 English abstract).

647 Molchanov, O. A., Kopytenko, Y. A., Voronov, P. M., Kopytenko, E. A., Matiashvili, T.
648 G., Fraser-Smith, A. C., and Bernardi, A.: Results of ULF Magnetic field
649 measurements near the epicenters of the Spitak ($M_s 6.9$) and Loma Prieta ($M_s 7.1$)
650 earthquakes: comparative analysis, *Geophys. Res. Lett.*, 19, 1495–1498, 1992.

651 Molchanov, O. A., Fedorov, E., Schekotov, A., Gordeev, E., Chebrov, V., Surkov,
652 V., ..., Biagi, P. F.: Lithosphere-atmosphere-ionosphere coupling as governing
653 mechanism for preseismic short-term events in atmosphere and ionosphere, *Natural
654 Hazards Earth Syst. Sci.*, 4, 757-767, 2004.

655 Namgaladze, A. A., Zolotov, O. V., Karpov, M. I., and Romanovskaya, Y. V.:
656 Manifestations of the earthquake preparations in the ionosphere total electron
657 content variations. *Natural Science*, 4(11), 848–855, 2012.

658 Ohta, K., Umeda, K., Watanabe, M. and Hayakawa, M.: Relationship between ELF
659 magnetic field and Taiwan earthquake. In *Lithosphere-Atmosphere-Ionosphere
660 Coupling* (eds M. Hayakawa and O. A. Molchanov), Terra Science Publishers,
661 Tokyo, pp. 233–237, 2002.

662 Panfilov, A. A.: The results of experimental studies of VLF–ULF electromagnetic

663 emission by rock samples due to mechanical action, *Nat. Hazards Earth Syst. Sci.*,
664 14, 1383–1389, doi:10.5194/nhess-14-1383-2014, 2014.

665 Park, S. K.: Precursors to earthquakes: seismo-electromagnetic signals, *Surv.*
666 *Geophys.*, 17, 493–516, 1996.

667 Pulinets, S. A., and Davidenko, D.: Ionospheric precursors of earthquakes and Global
668 Electric Circuit. *Advances in Space Research*, 53(5), 709–723, 2014.

669 Pulinets, S. A., and Ouzounov, D.: Lithosphere-Atmosphere-Ionosphere Coupling
670 (LAIC) model-An unified concept for earthquake precursors validation, *J.*
671 *Southeast Asian Earth Sci.*, 41(4–5): 371–382, 2011.

672 Pulinets, S. A., Boyarchuk, K. A., Hegai, V. V., Kim, V. P., and Lomonosov, A. M.:
673 Quasielectrostatic model of atmosphere-thermosphere-ionosphere coupling, *Adv.*
674 *Space Res.*, 26, 1209-1218, 2000.

675 Pulinets, S.A., Legen'ka, A.D., Alekseev, V.A., 1994. Pre-earthquakes effects and
676 their possible mechanisms. In: *Dusty and Dirty Plasmas, Noise and Chaos in Space*
677 *and in the Laboratory*. Plenum Publishing, New York, pp. 545–557.

678 Qian, S., Hao, J., Zhou, J. and Gao, J.: Precursory Electric and Magnetic Signals at
679 ULF and LF Bands during the Fracture of Rocks under Pressure. *Earthquake*
680 *Research in China*, 19(2), 109–116, 2003 (in Chinese with English abstract).

681 Qian, S., Hao, J., Zhou, J. and Gao, J.: Simulating experimental study on ULF
682 electromagnetic precursors before Jiji $M_s = 7.4$ earthquake. In
683 *Lithosphere-Atmosphere-Ionosphere Coupling* (eds Hayakawa, M. and Molchanov,
684 O. A.), Terra Science Publishers, Tokyo, pp. 49–53, 2002.

685 Qian, S., Ren K., Lü Z.: Experimental study on VLF, MF, HF and VHF
686 electromagnetic radiation characteristics with the rock breaking, *Earthquake*
687 *Science*, 18(3), 346–351, 1996 (in Chinese with English abstract).

688 Sarlis, N., Lazaridou, M., Kaporis, P., and Varotsos, P.: Numerical model of the
689 selectivity effect and the V/L criterion, *Geophys. Res. Lett.*, 26, 3245–3248, 1999.

690 Scoville, J., J. Sornette, and Freund, F. T.: "Paradox of peroxy defects and positive
691 holes in rocks Part II: Outflow of electric currents from stressed rocks." *Journal of*
692 *Asian Earth Sciences* 114, Part 2: 338-351, 2015.

693 Simpson, J. J., and Taflove, A.: Electrokinetic effect of the Loma Prieta earthquake
694 calculated by an entire-Earth FDTD solution of Maxwell's equations. *Geophys. Res.*
695 *Lett.*, 32, L09302, doi: 10. 1029/2005GL022601, 2005.

696 Sorokin, V. M., and Hayakawa, M.: Generation of Seismic-Related DC Electric
697 Fields and Lithosphere-Atmosphere-Ionosphere Coupling. *Modern Applied*
698 *Science*, 7(6), 1–25, 2013.

699 Sorokin, V. M., and Hayakawa, M.: Plasma and Electromagnetic Effects Caused by
700 the Seismic-Related Disturbances of Electric Current in the Global Circuit. *Modern*
701 *Applied Science*, 8(4), 61–83, 2014.

702 Uyeda, S., Nagao, T., Orihara, Y., Yamaguchi, T., and Takahashi I.: Geoelectric

703 potential changes: Possible precursors to earthquakes in Japan, *Proc. Nat. Acad.*
704 *Sci.*, 97, 4561–4566, 2000.

705 Varotsos, P., and Lazaridou, M.: Latest aspects of earthquake prediction in Greece
706 based on seismic electric signals. *Tectonophysics*, 188, 321–347, 1991.

707 Varotsos, P., Sarlis, N., and Lazaridou, M.: Transmission of stress induced electric
708 signals in dielectric media, Part II, *Acta Geophys*, 48, 141–177, 2000.

709 Varotsos, P., Sarlis, N., Skordas, E., Tanaka, H., and Lazaridou, M.: Additional
710 evidence on some relationship between seismic electric signals and earthquake
711 source parameters, *Acta Geophys.*, 53, 293–298, 2005.

712 Wait, J. R.: *Geo-electromagnetism*: Academic Press, 1982.

713 Wait, J. R.: Some Factors Concerning Electromagnetic Wave Propagation in the
714 Earth's Crust, *Proc. IEEE*, 54(8), August 1966.

715 Xu, C., Di, Q. Y., Fu, C. M. and Wang, M. Y.: The contrast of response
716 characteristics between large power long dipole and circle source, *Chinese J.*
717 *Geophys*, 55(6), 2097–2104, doi: 10. 6038/j. issn. 0001–5733. 2012. 06. 03, 2012,
718 (in Chinese with English abstract).

719 Xu, T., Hu, Y., Wu, J., Wu, Z., Suo, Y., and Feng, J.: Giant disturbance in the
720 ionospheric F2 region prior to the M8.0 Wenchuan earthquake on 12 May 2008,
721 *Ann. Geophys.*, 28, 1533–1538, 2010.

722 Xu, X. W.: *Album of 5.12 Wenchuan 8.0 earthquake surface ruptures*. Seismological
723 press, 2009 (in Chinese with English abstract).

724 Yamauchi, T., Maekawa, S., Horie, T., Hayakawa, M., and Soloviev, O.:
725 Subionospheric VLF/LF monitoring of ionospheric perturbations for the 2004
726 Mid-Niigata earthquake and their structure and dynamics, *J. Atmos. Sol. Terr.*
727 *Phys.*, 69, 793–802, 2007.

728 Yu, T., Mao, T., Wang, Y. G., and Wang, J. S.: Study of the ionospheric anomaly
729 before the Wenchuan earthquake, *Chinese Science Bulletin*, 54(6): 1086–1092, doi:
730 10.1007/s11434-008-0587-8, 2009 (in Chinese with English abstract).

731 Zeng, Z. C., Zhang, B., Fang, G. Y., Wang, D. F., and Yin, H. J.: The analysis of
732 ionospheric variations before Wenchuan earthquake with DEMETER data, *Chinese*
733 *J. Geophys.*, 52(1): 11–19, 2009 (in Chinese with English abstract).

734 Zhang, X., Shen, X., Liu, J., Ouyang, X., Qian, J., and Zhao, S.: Analysis of
735 ionospheric plasma perturbations before Wenchuan earthquake. *Nat. Hazards Earth*
736 *Syst. Sci.*, 9: 1259–1266, 2009.

737 Zhang, Y., Feng, W. P., Xu, L. S., Zhou, C. H., and Chen, Y. T.: Spatio-temporal
738 rupture process of the 2008 great Wenchuan earthquake, *Science in China Series D:*
739 *Earth Sciences*, 52 (2), 145–154, 2009.

740 Zhu, Y. T., Wang, X. B., Yu, N., Gao, S. Q., Li, K., and Shi, Y. J.: Longmenshan

741 magnetotelluric deep structure and the Wenchuan earthquake ($M_S8.0$), *Acta*
742 *Geologica Sinica*, 82 (12), 1769–777, 2008 (in Chinese with English abstract).
743 Zolotov, O. V.: Ionosphere Quasistatic Electric Fields Disturbances over Seismically
744 Active Regions as Inferred from Satellite-Based Observations: A Review. *Russian*
745 *Journal of Physical Chemistry B*, 9(5), 85–788, 2015.
746 Zolotov, O. V., Namgaladze, A. A., Zakharenkova, I. E., Martynenko, O. V.,
747 and Shagimuratov, I. I.: Physical Interpretation and Mathematical Simulation of
748 Ionospheric Precursors of Earthquakes at Midlatitudes. *Geomagnetism &*
749 *Aeronomy*, 52(3), 390–397, 2012.
750
751